An RNA-immunoprecipitation via CRISPR/dCas13 reveals an interaction between the SARS-CoV-2 5'UTR RNA and the process of human lipid metabolism.

Yurika Shimizu
Okayama University
Srinivas Bandaru
Kawasaki Medical School
Mari Hara
Kawasaki Medical School
Sonny Young
University of California San Francisco
Toshikazu Sano
University of California San Francisco
Kaya Usami
Okayama University
Yuta Kurano
Kawasaki Medical School
Suni Lee
Kawasaki Medical School
Naoko Kumagai-Takei
Kawasaki Medical School
Shunji Sano
University of California San Francisco
Tatsuo Ito (tataito@med.kawasaki-m.ac.jp)
Kawasaki Medical School

Research Article

Keywords: SARS-CoV-2 5'UTR, CRISPR/dCas13, RNA immunoprecipitation, Lipid Metabolism, Mevalonate pathway

Posted Date: May 14th, 2021

DOI: https://doi.org/10.21203/rs.3.rs-464458/v1

An RNA-immunoprecipitation via CRISPR/dCas13 reveals an interaction between the SARS-CoV-2 5'UTR RNA and the process of human lipid metabolism.

Yurika Shimizu[1,2], Srinivas Bandaru[1], Mari Hara[1], Sonny Young[3], Toshikazu Sano[3], Kaya Usami[4], Yuta Kurano[5], Suni Lee[1], Naoko Kumagai-Takei[1], Shunji Sano[3], Tatsuo Ito[1*]

1. Department of Hygiene, Kawasaki Medical School, 577 Matsushima, Kurashiki, Okayama, 701-0192, Japan.
2. Department of Pathophysiology, Periodontal Science, Okayama University Graduate School of Medicine, Dentistry, and Pharmaceutical Sciences, Okayama, Okayama, 700-8558, Japan.
3. Department of Surgery, Division of Pediatric Cardiothoracic Surgery, University of California San Francisco, San Francisco, CA, USA.
4. Okayama University Medical School, Okayama, 700-8558, Japan.
5. Kawasaki Medical School, 577 Matsushima, Kurashiki, Okayama, 701-0192, Japan.

*Corresponding author

Tatsuo Ito

Department of Hygiene,

Kawasaki Medical University, 577 Matsushima, Kurashiki, Okayama, 701-0192, Japan.

tataito@med.kawasaki-m.ac.jp.

Author Contributions

T.I.: Principal investigator of the project, conceptualized the idea, written original draft, performed formal analysis and generated figures

Y.S.: Co-investigated the project and helped in result validation.

S.B., M.H., S.Y., T.S., K.U.: Visualized the data and performed statistical analysis.

Y.K., S.L., N.K.T.: Validated and curated the data and additional programmer of the project.

S.S.: Chief project administrator.

CONFLICT OF INTEREST

The authors declare no conflict of interest.

Abstract

We herein elucidate the function of SARS-CoV-2 derived 5'UTR in the human cells. 5'UTR bound cellular RNA was immunoprecipitated by gRNA-dCas13 targeting luciferase RNA fused to SARS-CoV-2 5'UTR in HEK293T and A549 cells. The 5'UTR bound RNA extractions were predominantly enriched for regulating lipid metabolism. Overexpression of SARS-CoV-2 5'UTR RNA altered the expression of factors known to be involved in the process of the human Mevalonate pathway. Besides, HMMG-CoA reductase inhibitors suppressed 5'UTR-mediated translation activity, which is derived from the SARS-CoV-2 model. In conclusion, we deduce the array of host RNAs interacting with SARS-CoV-2 5'UTR that drives SARS-CoV-2 translational initiation and influences metabolic pathways.

Keywords: SARS-CoV-2 5'UTR, CRISPR/dCas13, RNA immunoprecipitation, Lipid Metabolism, Mevalonate pathway

Introduction

The outbreak of a novel strain of coronavirus — SARS-CoV-2 causing severe respiratory illness designated as COVID-19, surged as a large-scale global pandemic claiming more than 1 million lives while requiring intensive care hospitalizations for about 2% to 10% of the infected cases worldwide [1]. Accumulated data corroborated since a year of the pandemic has shown COVID-19 patients to present diverse symptoms with severe immune dysregulation of unknown incentives [2-5].

It is noteworthy that a recent meta-analysis establishes a positive link between COVID-19 vulnerability with obesity [6 -10]. Hospital-based studies showed that people with obesity were 113% more likely to contract SARS-CoV-2 and 74% of them required intensive care admissions [11]. Furthermore, patients in the excessive BMI range with metabolic-related fatty liver disease demonstrated an enhanced risk of severe COVID-19 disease [12]. These

studies explicitly indicate obesity as a potential comorbid condition for COVID-19 affecting the overall course of the disease by influencing viral load, tissue damage, and mortality.

Genome sequencing with a phylogenetic classification revealed that SARS-CoV-2 belongs to β genus of coronavirus sharing 96% homologous to bat-derived SARS-like viruses [13,14]. Although the rate of mutation in SARS-CoV-2 is slow (two single nucleotide substitutions per month) [15], nevertheless, more than 12,000 mutations have been documented so far (www.gisaid.org). Among these, only a few of them result in the virus's protein variations which make it competent for human-to-human transmission.

The SARS-CoV-2 genome is a positive-strand RNA molecule (+) ssRNA characterized by open reading frames - ORF1a and ORF1b and conserved consensus for coding structural/accessory proteins [16]. Following viral invasion into the host cell, translation of ORF1a and ORF1b from the entire ss (+) RNA marks the first event of the infectious process [17]. SARS-CoV-2 genomic RNA is capped at the 5'end, and translation initiation efficiency is regulated by a stable hairpin structure near the cap structure [18,19].

In the present study, we investigate host factors responsible for SARS-CoV-2 translation by CRISPR/dCas13 aided targeting of SARS-CoV-2 5'UTR followed by analysis of trans immunoprecipitated 5'UTR bound host RNAs of human cells.

Results

Selection of high prevalent 5'UTR region of SARS-CoV-2.

In order to understand the translation regulation of SARS-CoV-2 genome, we introduced the 5’UTR leader sequence of SARS-CoV-2 into the host cell (A549 and HEK293T cells). This region is important to facilitate understanding of (1) the array of host RNAs that would bind to 5’UTR leader in regulating translation of the viral genome and (2) the host cell types that are more susceptible for SARS-CoV-2 infection and replication. However, considering the fact that hypermutation in 5’UTR regions is typical to viral genomes it was essential to use only those 5’UTRs in the present experiment which have large geographic expansions i.e. prevalent across the diverse ethnicities and conserved since the first outbreak.

Numerous reports have been made on sequence variation and phylogenetics of SARS-CoV-2, and they are constantly updated on Nextstrain.org. Shown here in a data snapshot containing a quality filtered subset of 3,935 available data points from the site. Among the 264nt sequences in the 5'UTR region of SARS-CoV-2, the one derived from the 241C> T point mutation was proven to be the most prevalent in almost all the infected cases worldwide. Interestingly, the 241T mutant was also detected at the first outbreak in Wuhan China in 2019. While other 5'UTR mutations, although been reported, did not lead to clade formations. The rationale for the high prevalence of 241T mutant still remains elusive. Presumably, it may benefit viral survival and replication in host cells. Given this literature, we hence selected 5'UTR sequence for our study and henceforth identify the cluster of host RNAs that bind to this 5'UTR and aid translation regulation of SARS-CoV-2 genome in human cells. The complete workflow of this study is demonstrated in **Figure 1.**

Translation activation by 5'UTR RNA derived from SARS-CoV-2.

The sequence of the 5'UTR region of SARS-CoV-2 (isolated from the Wuhan-Hu-1 genome (NC_045512)) was oligo-synthesized. The synthesized sequence was cloned in Luciferase reporter pGL3-Promoter Vector (Promega: E1761) specifically between SV40 promoter sequence and luciferase gene sequence to express the 5'UTR-fused-luciferase RNA (**Figure 2-a**). This bonafide vector was introduced into human cell lines HEK293T and A549 with a concentration gradient, and the expression was measured as a function of luminescence from the translation of luciferase protein. Interestingly, luciferase RNA fused to SARS-CoV-2-derived 5'UTR showed stronger luciferase activity in HEK293T cells and A549 cells in contrast to cells expressing luciferase RNA alone. (**Figure 2-b**) The improved translation efficiency suggests a favorable translational activity of SARS-CoV-2-derived 5'UTR in the human intracellular environment.

gRNA-dCas13 assisted Trans RNA Immunoprecipitation (TRIP) of host regulatory RNA bound to 5'UTR of SARS-CoV-2.

Our next pursuit was to determine the cluster of cellular RNAs that regulate SARS-CoV-2 genome by allosteric binding at 5'UTR sequence. To achieve this, we first predicted the structure of 5'UTR fused luciferase RNA, and confirmed that 5'UTR RNA formed a secondary structure independent of luciferase RNA. Next, in order to pull down host RNAs bound to 5' UTR we targeted luciferase fraction of 5'UTR-lucefierase fused RNA by gRNA-dCas13 for RNA Trans immunoprecipitation (TRIP). We designed two candidate single-strand regions for designing guide RNAs (gRNA) in the luciferase RNA. The gRNAs targeting these regions were named Luc1 and Luc2, respectively (**Figure 3-a**). The dCas13 gene sequence was inserted into the AAVS1 gene region of HEK293T cells and A549 cells by homologous recombination, followed by the selection of vector inserted cells with 10ug/ml puromycin for 24hour incubation. Next, lentivirus vectors expressing RFP and Luc1-gRNA or Luc2-gRNA were inserted in each cell, and the cells expressing RFP were collected by cell sorting. In the following experiment, we induced pGL3-5'UTR vector or pGL3-promoter vector into cell lines expressing dCas13 and Luc1-gRNA or Luc2-gRNA, and performed RNA Immunoprecipitation (RIP) using AM-Tag antibody (pAb) (ActiveMotif: 61678). With qPCR we confirmed that the immunoprecipitated RNA libraries

contained transcribed SARS-CoV-2-derived 5'UTR RNA and/or luciferase RNA. SARS-CoV-2 derived 5'UTR RNA and luciferase RNAs were not detected in cells expressing gRNA that do not target luciferase RNA (nontarget gRNA) (**Figure 3-b**). Hence we achieved the extraction of 5' UTR bound host RNA clusters that are crucial in the translation of SARS-CoV-2 genome by gRNA-dCas13 assisted Trans RNA Immunoprecipitation (TRIP) method.

5'UTR bound host regulatory RNA predominantly contains genes for lipid metabolism

Host regulatory RNA bound to 5'UTR extracted from TRIP were then subjected to ultra-low input RNA sequencing. In the cluster analysis of differentially enriched genes, we found that the RNA group that binds to SARS-CoV-2 5'UTR RNA in A549 cells belong to a different cluster for the RNA group that binds to Luciferase RNA. (**Figure 4-a**). Similar enrichment differences between RNA group that binds to the 5'UTR RNA of SARS-CoV-2 and the control group that binds only to the RNA of luciferase could be confirmed in HEK293T cells as well. (We confirmed the duplication of genes that are differentially enriched in each group

compared to the control group or genes that are differentially enriched in multiple groups). We found that more than 1,000 RNA genes that bind to the 5'UTR of SARS-CoV-2 are shared between A549 cells and HEK293T cells. (**Figure 4-b**). Further, we performed Gene Ontology enrichment analysis of RNA genes that bind predominantly (p-value <0.01) to 5'UTR of SARS-CoV-2 extracted from HEK293T cells and A549. The top 5 GO terms identified in the analysis were lipid metabolic process, the cellular lipid metabolic process, the small molecule metabolic process, the organic acid metabolic process and oxoacid metabolic process. (**Figure 4-c & Table 1**). These results suggest that the 5'UTR of SARS-CoV-2 may interfere significantly with lipid metabolism in human cells.

Next, we performed peak calling followed by motif analysis for 5'UTR bound host RNA which enabled us to identify protein binding regions (**Figure 5 & Table 2**). From the concentrated RNA motif, respectively 12 and 14 types of RNA-binding proteins were extracted from HEK293T and A549 cells. The proteins commonly observed in both cells were RBM38, BRUNOL4, BLUNOL5, and TARDBP. All of them are essentially metabolic regulators. This observation suggests that the SARS-CoV-2 5'UTR may alter the cellular metabolic process, especially the lipid metabolic process in the host. We found that the

SARS-CoV-2 virus uses 5'UTR to interact with various protein and regulatory RNAs to *sneak* into the human intracellular environment for its translation initiation. It may be thought of as "*the takeover of RNA metabolism*" mechanism in the human cell by the SARS-CoV-2 virus.

5'UTR-mediated translation influences Mevalonate pathway

Following our previous investigation which showed that 5'UTR bound RNAs were enriched for lipid metabolism, we further examined whether factors for lipid metabolism altered upon entry of SARS-CoV-2 into the human cells. Therefore, we introduced pGL3-5'UTR or pGL3-Promoter vectors into HEK293T cells and A549 cells, and quantified the RNAs with qPCR. Surprisingly, significant changes in the mRNA expression level were observed for *ACAA*, *HMGCS*, and *FADS2* genes which are enriched in the Mevalonate pathway, and remarkably, *HMGCS* expression was highly upregulated (**Figure 6-a**). Since we had a set of enriched genes that bind to 5'UTR of SARS-CoV-2 in human cells, we further proceeded for drug repositioning by target identification. We used TargetMine program (https://targetmine.mizuguchilab.org) which aided the identification of suitable targets. As a

189 result, four interacting compounds (Atorvastatin, Simvastatin, Rosuvastatin and Pravastatin)
190 that can be expected to act (p-value<0.05) on the enriched RNA were identified. Amongst
191 all, statins (p-value <0.01) have been identified as optimal, ready-to-use compounds to treat
192 antiviral growth in COVID-19 patients. (**Figure 6-b**). To investigate, whether suppression of
193 translational activity by 5'UTR of SARS-CoV-2 can be induced, we added over-the-counter
194 drug HMG-CoA reductase inhibitors after overexpressing the pGL3-5'UTR or pGL3-
195 Promoter vector into HEK293T cells and A549 cells. It was interesting to observe that 5'UTR
196 SARS-CoV-2-mediated translational activity in both HEK293T cells and A549 cells were
197 significantly suppressed upon treatment with 100nM Atorvastatin (**Figure 6-c**). In addition,
198 in HEK293T cells, a translation inhibitory effect was observed upon treatment with 100nM
199 Rosuvastatin. (**Result not shown**). Since both Atorvastatin and Rosuvastatin are hydrogen-
200 bonded to Ser565 of HMG CoA, it is thought that they have an auxiliary effect that other
201 drugs do not have, which may be one of the reasons for their efficacies. Although there are
202 few reports on the relationship between the mevalonate pathway and viral infection, previous
203 reports have shown that suppressing HMGCS2 or ACAA2 expression may suppress
204 papillomavirus or poxvirus infection [20, 21]. Overall, our study predicts host RNA-binding

proteins crucial for SARS-CoV-2 translational initiation and regulation. Elucidation of transcriptional regulation of HMGCS2 or ACAA2 and its chaperone network including the results obtained from the present study provides multiple antiviral drug development opportunities.

Discussion

Since the outbreak of the COVID-19 pandemic in December 2019, its underlying molecular pathogenesis and clinical complications following the SARS-CoV-2 infection have been unceasingly investigated. Previous studies have shown that the COVID-19 patients suffer from excessive immune response termed "*cytokine storm*" with infiltration of cytokines, mononuclear cells, and monocytes [22-24]. However, in patients with bariatric diseases, the infiltration is extreme and prolonged, and it leads to acute tissue damage resulting in respiratory distress syndrome (ARDS) [7-9]. Our *in vitro* investigation supports the above clinical observation. Wherein we found significant dysregulation of lipid metabolism in cells treated with 5'UTR of SARS-CoV-2. It remains obscure why lipid metabolism is dysregulated upon SARS-CoV-2 infection making obese people more vulnerable to disease.

However two studies suggest preferential loss of lipids and amino acids was associated with enhanced infiltration of cytokines leading to disease severity in COVID-19 [25, 26]. It is anticipated that further understanding of altered lipid metabolism in the virus-infected cells may help uncover the severity pattern in patients.

Recent structural and biochemical insights have shown 10- to 20-fold higher affinity of SARS-CoV-2 spike proteins to human ACE2 receptors than SARS-CoV [27] which possibly explain the higher transmissibility of COVID-19 [28]. Therefore, an antibody-based therapeutic strategy that blocks the interaction site of SARS-CoV-2 and ACE2 receptor is anticipated to be effective [29]. Further, retroviral therapies including Ribavirin, favipiravir, and protease inhibitors such as lopinavir-ritonavir have been administered for clinical treatment of the infection. [30]. However the clinical efficacy of the aforementioned treatment still remains debatable. In any case, providing preliminary supportive care to the patients forms the effective disease management approach during the growing pandemic. Drug repositioning forms the rescue approach until a safe and reliable cure becomes available.

In the current study, we followed a similar approach of drug repositioning by proposing HMG-CoA reductases as an efficient treatment approach especially in obesity-related COVID-19 infections. We created an infection model for COVID-19 by introducing luciferase RNA fused with 5'UTR of SARS-CoV-2 into cell lines. Elucidating the function of the 5'UTR region stands important as it forms the translational initiation region for host cellular factors to translate SARS-CoV-2 RNA. In our investigation, the 5'UTR fusion luciferase showed strong translational activity and in particular, we observed significant changes in expression for genes related to mevalonate pathways and lipid metabolism. We herein show that HMG-CoA reductase inhibitors like Atorvastatin suppress the translational activation function of the 5'UTR region. Our cell-based investigation interestingly finds a good correlation with the previous clinical studies which showed that patients under the administration of HMG-CoA reductase inhibitors showed less aggravated symptoms for COVID-19 [31-33]. We anticipate that short-term administration of HMG-CoA reductase inhibitors may be more likely to suppress the exacerbation of SARS-CoV-2 infected individuals.

In conclusion, we emphasize that elucidating the function of the SARS-CoV-2 5'UTR region in human cells helps the understanding of the host transcriptome changes which may help to predict the severity of the infection. We also anticipate the dysregulated genes as a result of infection may serve as a biomarker to predict the course of the disease. Our CRISPR / dCas13-based RNA genetic engineering approach as employed in the present study can also be extended to understand host cell response in other infectious diseases as well.

Materials and methods

Cell culture and transfection

HEK293T (ATCC CRL-3216) was a gift from M. Ladanyi (Memorial Sloan Kettering Cancer Center, New York) and A549(ATCC CCL-185) cells was a gift from T. Takarada (Okayama University, Japan). These cells were grown in Dulbecco's modified Eagle's medium (Cellgro, D5796, Mediatech, Washington, DC) supplemented with 10% fetal calf serum and penicillin/streptomycin (Sigma). Plasmids were transfected into cells with GeneJammer (Agilent, 204130, Santa Clara, California, USA) according to the manufacturer's protocol. All cell lines and the plasmid containing the SARS-CoV-2 viral

genomic sequence were handled according to a protocol approved by the internal review committee and the ethics committee of Kawasaki Medical School and confirmed by the Minister of Education, Culture, Sports, Science and Technology of Japan (Accepted No.1020). We have NOT conducted experiments on any of the following which requires ethical clearances. (1) human embryos and gametes, (2) human embryonic stem cells and related materials, (3) clinical applications of stem cell, (4) Human recipients or donors of cells or tissue and (5) Animals experiment.

Plasmid preparation

Plasmids encoding human optimized dCas13 (full-length, following the am tag array with AM tag sequence: ATGTGCCAAGATCCTCAACGCAAAGGCAACGTGATACTCTCTCAGGCTTACGG GTGCCAAGATCCTCAACGCAAAGGCAACGTGATACTCTCTCAGGCTTAC) vector pENTR-dCas13 and crRNA backbone vector (pLKO5.U6.crRNA.tRFP.v1) were synthesized at GenScript (https://www.genscript.com/). pGL3-5'UTR reporter plasmid containing 5'UTR sequence of the SARS-CoV-2 was also synthesized at GenScript and

ligated into pGL3-promoter vector (Promega, E1761 ,Madison, Wisconsin, USA). Luc1-crRNA and Luc2-crRNA were constructed using BsmBI fragments sub-cloned into crRNA backbone vector pLKO5.U6.crRNA.tRFP.v1.

Trans RNA immunoprecipitation (TRIP)

Nuclear extracts from cell lines previously fixed with 2% paraformaldehyde were used for immunoprecipitation using 30 μl of anti-AM tag antibody (Active Motif, 61677, Carlsbad, California, USA). RNA immunoprecipitation was performed as described previously [26] except that the AM-tag fused dCas13-RNA complexes were eluted from the Protein A Dynabeads (Thermo Fisher Scientific,10001D, Waltham, Massachusetts, USA) and treated with 20 μg of proteinase K at 45 °C for 1 h, then de-crosslinked at 65 °C for 1 h. The RNA was isolated using TRI reagent (Ambion, AM9738, Austin, Texas, USA) according to the manufacturer's instructions. After treatment with Turbo DNase (Ambion, AM2238), the RNAs were subjected to RT-qPCR using primers to detect RNA sequence of Luciferase and 5'UTR of SARS-CoV-2. The RNAs were further subjected to Ultra Low Input RNA-seq

(GeneWiz, https://www.genewiz.com). The DNase treatment of the extracts was performed at 25 °C for 30 min using 20 U of Turbo DNase (Ambion, AM2238).

Quantitative polymerase chain reaction

Poly(A)'RNA and total RNA were extracted from HEK293T and A549 using the RNeasy mini kit (Qiagen, 74104, Hilden, Germany). cDNA was prepared by reverse transcription of 500 ng of total RNA using the PrimeScrip RT Master Mix (Takara, RR036A, Kusatsu, Japan). The resulting cDNAs were amplified using the QuantiTect SYBR Green PCR kit (Qiagen, 204143). The RT-PCR reaction was performed on StepOne Real-Time PCR Systems (Applied Biosystems, Foster City, California, USA). Quantitation, and calling of real-time amplification values were performed on StepOne Software Version 2.2 (https://www.thermofisher.com/). Expression data was normalized to glyceraldehyde-3-phosphate dehydrogenase (GAPDH) expression to the corresponding sample.

Luciferase Reporter Assay

pGL3-promoter vector and pGL3-5'UTR vector were used as a reporter gene for investigating the 5'UTR dependent translation activity. Plasmids were transiently transfected into HEK293T and A549 cells. The cells were harvested for 48 h after transfection, and then the luciferase activity was analyzed with Dual-Luciferase reporter assay system (Promega, E1910). Luciferase activity and reporter activities were normalized in reference to cotransfected Rous sarcoma virus (RSV)-galactosidase expression plasmid as described previously [34].

Drug-induced translation suppression

For translation suppression effect induced by HMG-CoA reductase inhibitors, cells were maintained in the presence or absence of Atorvastatin Calcium, Simvastatin, Rosuvastatin Calcium Salt, Pravastatin Sodium Salt (FUJIFILM Wako Chemicals, 1044516, 79902-63-9, 187-03361, 162-19821, Osaka, Japan) diluted in DMSO (1 nM - 1,000nM) for 48h

RNA seq and data analysis

329 Total RNA was sequenced on illumina NovaSeq 6000 sequencing platform on a 2x150 bp
330 flow cell. Reads generated from sequencing were saved in Illumina specific (Binary Base
331 Call (BCL) file format. All the BCL files were converted to fastq files with Bcl2fastq
332 v2.17.1.14 (https://sapac.support.illumina.com/downloads/bcl2fastq-conversion-software-
333 v2-20.html) compatible for downstream sequence analysis programs. Prior to data analysis,
334 the reads were filtered by eliminating low-quality reads (Phred score <30) by FastQC
335 (http://www.bioinformatics.babraham.ac.uk/projects/fastqc/), trimming reads those less than
336 75 bp by Trinnomatic v 0.36 (http://www.usadellab.org/cms/index.php?page=trimmomatic)
337 [35] cutting adapter sequences by Cutadapt version 1.9.1
338 (https://cutadapt.readthedocs.io/en/v1.9.1/) [36]. The filtered reads were subsequently
339 aligned to the Human reference GRCh38.p12 using Hisat2 v2.0.1 [37] followed by assigning
340 the reads onto genomic features – exons, introns and intergenic regions. The mapped reads
341 were visualized by Integrative Genomics Viewer Version 2.5.2
342 (https://software.broadinstitute.org/software/igv/) [38]. For assembly and predict alternative
343 splicing StringTie v1.3.3b (https://ccb.jhu.edu/software/stringtie/) [39] was used and
344 ASprofile V1.0.4 (https://ccb.jhu.edu/software/ASprofile/) [40] was employed for

345 classification and quantification of the spliced reads[6]. For de novo transcript assembly
346 StringTie v1.3.3b was employed using the alignment bam files, the result of which was then
347 subjected to comparison with existing annotation reference (gtf file) using Cuffcompare
348 V2.2.1 (https://www.genepattern.org/modules/docs/Cufflinks.cuffcompare/7) [41] .
349 Gene_expression calculation was performed as a function of FPKM with a threshold of 0.1-
350 1 based on read counts from HT-seq v
351 0.6.1(https://bioweb.pasteur.fr/packages/pack@HTSeq@0.6.1) [42]. Differential gene
352 analysis was performed using the Bioconductor package DESeq2 V1.6.3 and edgeR V3.4.6
353 (https://bioconductor.org/packages/release/bioc/html/edgeR.html) [43]. The results from
354 EdgeR analysis were further analyzed to determine genes with significant differential
355 expression according to the criteria of fold change greater than 2 and qvalue (fdr, padj) less
356 than 0.05. The GO functional enrichment analysis was performed by GOSeq 1.42.0
357 (https://bioconductor.org/packages/release/bioc/html/goseq.html) [44]. TopGO
358 (https://bioconductor.org/packages/release/bioc/html/topGO.html) [45] was applied for
359 generating Directed Acyclic Graph (DAG) for results of enrichment analysis of the
360 differentially expressed genes. To assess differential expression of exons and alternative exon

usage in alternative splicing DEXSeq (V1.18.4) (https://www.rdocumentation.org/packages/DEXSeq/versions/1.18.4) was used [46].

References

1. Iype, Eldhose, and Sadhya Gulati. "Understanding the asymmetric spread and case fatality rate (CFR) for COVID-19 among countries." *medRxiv* (2020).
2. Chen, N., Zhou, M., Dong, X., Qu, J., Gong, F., Han, Y., ... & Zhang, L. (2020). Epidemiological and clinical characteristics of 99 cases of 2019 novel coronavirus pneumonia in Wuhan, China: a descriptive study. *The lancet*, *395*(10223), 507-513.
3. Buonsenso, D., Piano, A., Raffaelli, F., Bonadia, N., Donati, K. D. G., & Franceschi, F. (2020). Novel coronavirus disease-19 pnemoniae: a case report and potential applications during COVID-19 outbreak. *European review for medical and pharmacological sciences*, *24*, 2776-2780.
4. Zhang, J. J., Dong, X., Cao, Y. Y., Yuan, Y. D., Yang, Y. B., Yan, Y. Q., ... & Gao, Y. D. (2020). Clinical characteristics of 140 patients infected with SARS-CoV-2 in Wuhan, China. *Allergy*, *75*(7), 1730-1741.
5. Wang, C., Horby, P. W., Hayden, F. G., & Gao, G. F. (2020). A novel coronavirus outbreak of global health concern. *The lancet*, *395*(10223), 470-473.

6. Honce, R., Karlsson, E. A., Wohlgemuth, N., Estrada, L. D., Meliopoulos, V. A., Yao, J., & Schultz-Cherry, S. (2020). Obesity-related microenvironment promotes emergence of virulent influenza virus strains. *MBio*, *11*(2).
7. Huttunen R, Syrjanen J. Obesity and the risk and outcome of infection. Int J Obes. 2013;37:333–40.
8. Jones, C. Y., Hogan, J. W., Snyder, B., Klein, R. S., Rompalo, A., Schuman, P., ... & HIV Epidemiology Research Study Group. (2003). Overweight and human immunodeficiency virus (HIV) progression in women: associations HIV disease progression and changes in body mass index in women in the HIV epidemiology research study cohort. *Clinical Infectious Diseases*, *37*(Supplement_2), S69-S80.
9. Falagas, M. E., Athanasoulia, A. P., Peppas, G., & Karageorgopoulos, D. E. (2009). Effect of body mass index on the outcome of infections: a systematic review. *Obesity reviews*, *10*(3), 280-289.
10. Muscogiuri, G., Pugliese, G., Barrea, L., Savastano, S., & Colao, A. (2020). Comentary: obesity: the "Achilles heel" for COVID-19?. *Metabolism-Clinical and Experimental*, *108*.
11. Popkin, B. M., Du, S., Green, W. D., Beck, M. A., Algaith, T., Herbst, C. H., ... & Shekar, M. (2020). Individuals with obesity and COVID-19: A global perspective on the epidemiology and biological relationships. *Obesity Reviews*, *21*(11), e13128.
12. Dietz, W., & Santos-Burgoa, C. (2020). Obesity and its implications for COVID-19 mortality. *Obesity*, *28*(6), 1005-1005.

13. Zhu, N., Zhang, D., Wang, W., Li, X., Yang, B., Song, J., ... & Tan, W. (2020). A novel coronavirus from patients with pneumonia in China, 2019. *New England journal of medicine*.

14. Zhou, P., Yang, X. L., Wang, X. G., Hu, B., Zhang, L., Zhang, W., ... & Shi, Z. L. (2020). A pneumonia outbreak associated with a new coronavirus of probable bat origin. *nature*, *579*(7798), 270-273.

15. Hodcroft, E. B., Zuber, M., Nadeau, S., Crawford, K. H., Bloom, J. D., Veesler, D., ... & Neher, R. A. (2020). Emergence and spread of a SARS-CoV-2 variant through Europe in the summer of 2020. *MedRxiv*.

16. Wu, A., Peng, Y., Huang, B., Ding, X., Wang, X., Niu, P., ... & Jiang, T. (2020). Genome composition and divergence of the novel coronavirus (2019-nCoV) originating in China. *Cell host & microbe*, *27*(3), 325-328.

17. Plant, E. P., Rakauskaitė, R., Taylor, D. R., & Dinman, J. D. (2010). Achieving a golden mean: mechanisms by which coronaviruses ensure synthesis of the correct stoichiometric ratios of viral proteins. *Journal of virology*, *84*(9), 4330-4340.

18. Miao, Z., Tidu, A., Eriani, G., & Martin, F. (2020). Secondary structure of the SARS-CoV-2 5'-UTR. *RNA biology*, 1-10.

19. Babendure, J. R., Babendure, J. L., Ding, J. H., & Tsien, R. Y. (2006). Control of mammalian translation by mRNA structure near caps. *Rna*, *12*(5), 851-861.

20. Filone, C. M., Caballero, I. S., Dower, K., Mendillo, M. L., Cowley, G. S., Santagata, S., ... & Connor, J. (2014). The master regulator of the cellular stress response (HSF1) is critical for orthopoxvirus infection. *PLoS Pathog*, *10*(2), e1003904.

21. Lipovsky, A., Popa, A., Pimienta, G., Wyler, M., Bhan, A., Kuruvilla, L., ... & DiMaio, D. (2013). Genome-wide siRNA screen identifies the retromer as a cellular entry factor for human papillomavirus. *Proceedings of the National Academy of Sciences*, *110*(18), 7452-7457.

22. Diao, B., Feng, Z., Wang, C., Wang, H., Liu, L., Wang, C., ... & Chen, Y. (2020). Human kidney is a target for novel severe acute respiratory syndrome coronavirus 2 (SARS-CoV-2) infection. *MedRxiv*.

23. Zheng, H. Y., Zhang, M., Yang, C. X., Zhang, N., Wang, X. C., Yang, X. P., ... & Zheng, Y. T. (2020). Elevated exhaustion levels and reduced functional diversity of T cells in peripheral blood may predict severe progression in COVID-19 patients. *Cellular & molecular immunology*, *17*(5), 541-543.

24. Mehta, P., McAuley, D. F., Brown, M., Sanchez, E., Tattersall, R. S., & Manson, J. J. (2020). COVID-19: consider cytokine storm syndromes and immunosuppression. *The lancet*, *395*(10229), 1033-1034.

25. Alqahtani, S. A., & Schattenberg, J. M. (2020). Liver injury in COVID-19: The current evidence. *United European gastroenterology journal*, *8*(5), 509-519.

438 26. Cecere, G., Hoersch, S., Jensen, M. B., Dixit, S., & Grishok, A. (2013). The ZFP-1
439 (AF10)/DOT-1 complex opposes H2B ubiquitination to reduce Pol II
440 transcription. *Molecular cell*, *50*(6), 894-907.
441 27. Wan, Y., Graham, R., Baric, R., & Li, F. (2020). An analysis based on decade-long
442 structural studies of SARS 3, JVI Accepted Manuscript Posted Online 29 January
443 2020. *J. Virol*.
444 28. Bourgonje, A. R., Abdulle, A. E., Timens, W., Hillebrands, J. L., Navis, G. J., Gordijn,
445 S. J., ... & van Goor, H. (2020). Angiotensin-converting enzyme 2 (ACE2), SARS-
446 CoV-2 and the pathophysiology of coronavirus disease 2019 (COVID-19). *The*
447 *Journal of pathology*, *251*(3), 228-248.
448 29. Gue, Y. X., Kanji, R., Markides, V., & Gorog, D. A. (2020). Angiotensin Converting
449 Enzyme 2 may mediate disease severity in COVID-19. *American Journal of*
450 *Cardiology*, *130*, 161-162.
451 30. Zumla, A., Chan, J. F., Azhar, E. I., Hui, D. S., & Yuen, K. Y. (2016).
452 Coronaviruses—drug discovery and therapeutic options. *Nature reviews Drug*
453 *discovery*, *15*(5), 327-347.
454 31. Tan, W. Y., Young, B. E., Lye, D. C., Chew, D. E., & Dalan, R. (2020). Statin use is
455 associated with lower disease severity in COVID-19 infection. *Scientific*
456 *reports*, *10*(1), 1-7.
457 32. Song, S. L., Hays, S. B., Panton, C. E., Mylona, E. K., Kalligeros, M., Shehadeh, F.,
458 & Mylonakis, E. (2020). Statin use is associated with decreased risk of invasive

459 mechanical ventilation in COVID-19 patients: a preliminary study. *Pathogens*, *9*(9),
460 759.
461 33. De Spiegeleer, A., Bronselaer, A., Teo, J. T., Byttebier, G., De Tré, G., Belmans, L., ...
462 & De Spiegeleer, B. (2020). The effects of ARBs, ACEis, and statins on clinical
463 outcomes of COVID-19 infection among nursing home residents. *Journal of the*
464 *American Medical Directors Association*, *21*(7), 909-914.
465 34. Tsuda, M., Takahashi, S., Takahashi, Y., & Asahara, H. (2003). Transcriptional co-
466 activators CBP/p300 regulates chondrocyte specific gene expression via association
467 with Sox9. *Journal of Biological Chemistry*.
468 35. Bolger, A. M., Lohse, M., & Usadel, B. (2014). Trimmomatic: a flexible trimmer for
469 Illumina sequence data. *Bioinformatics*, *30*(15), 2114-2120.
470 36. Martin, M. (2011). Cutadapt removes adapter sequences from high-throughput
471 sequencing reads. *EMBnet. journal*, *17*(1), 10-12.
472 37. Kim, D., Paggi, J. M., Park, C., Bennett, C., & Salzberg, S. L. (2019). Graph-based
473 genome alignment and genotyping with HISAT2 and HISAT-genotype. *Nature*
474 *biotechnology*, *37*(8), 907-915.
475 38. Robinson, J. T., Thorvaldsdóttir, H., Winckler, W., Guttman, M., Lander, E. S., Getz,
476 G., & Mesirov, J. P. (2011). Integrative genomics viewer. *Nature*
477 *biotechnology*, *29*(1), 24-26.

478 39. Kovaka, S., Zimin, A. V., Pertea, G. M., Razaghi, R., Salzberg, S. L., & Pertea, M.
479 (2019). Transcriptome assembly from long-read RNA-seq alignments with
480 StringTie2. *Genome biology*, *20*(1), 1-13.
481 40. Florea, L., Song, L., & Salzberg, S. L. (2013). Thousands of exon skipping events
482 differentiate among splicing patterns in sixteen human tissues. *F1000Research*, *2*.
483 41. Trapnell, C., Williams, B. A., Pertea, G., Mortazavi, A., Kwan, G., Van Baren, M.
484 J., ... & Pachter, L. (2010). Transcript assembly and quantification by RNA-Seq
485 reveals unannotated transcripts and isoform switching during cell
486 differentiation. *Nature biotechnology*, *28*(5), 511-515.
487 42. Anders, S., Pyl, P. T., & Huber, W. (2015). HTSeq—a Python framework to work
488 with high-throughput sequencing data. *Bioinformatics*, *31*(2), 166-169.
489 43. Robinson, M. D., McCarthy, D. J., & Smyth, G. K. (2010). edgeR: a Bioconductor
490 package for differential expression analysis of digital gene expression
491 data. *Bioinformatics*, *26*(1), 139-140.
492 44. Young, M. D., Wakefield, M. J., Smyth, G. K., & Oshlack, A. (2010). Gene ontology
493 analysis for RNA-seq: accounting for selection bias. *Genome biology*, *11*(2), 1-12.
494 45. Alexa, A., & Rahnenfuhrer, J. (2020). TopGo: Enrichment Analysis for Gene
495 Ontology; R Package Version 2.42. 0. 2020.
496 46. Anders, S., Reyes, A., & Huber, W. (2012). Detecting differential usage of exons
497 from RNA-seq data. *Nature Precedings*, 1-1.
498

List of Figures

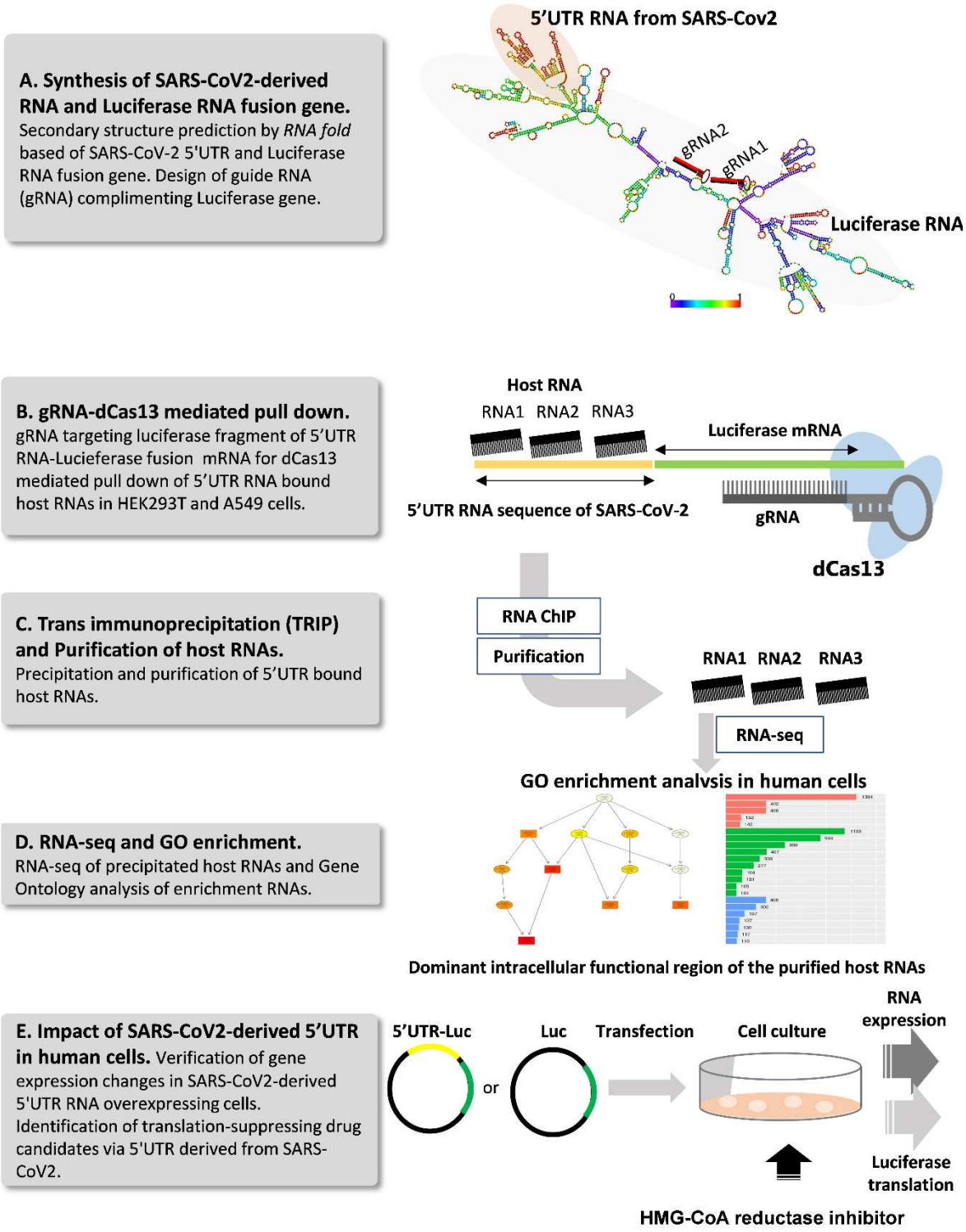

508

509 **Figure 1. Workflow of the study.**

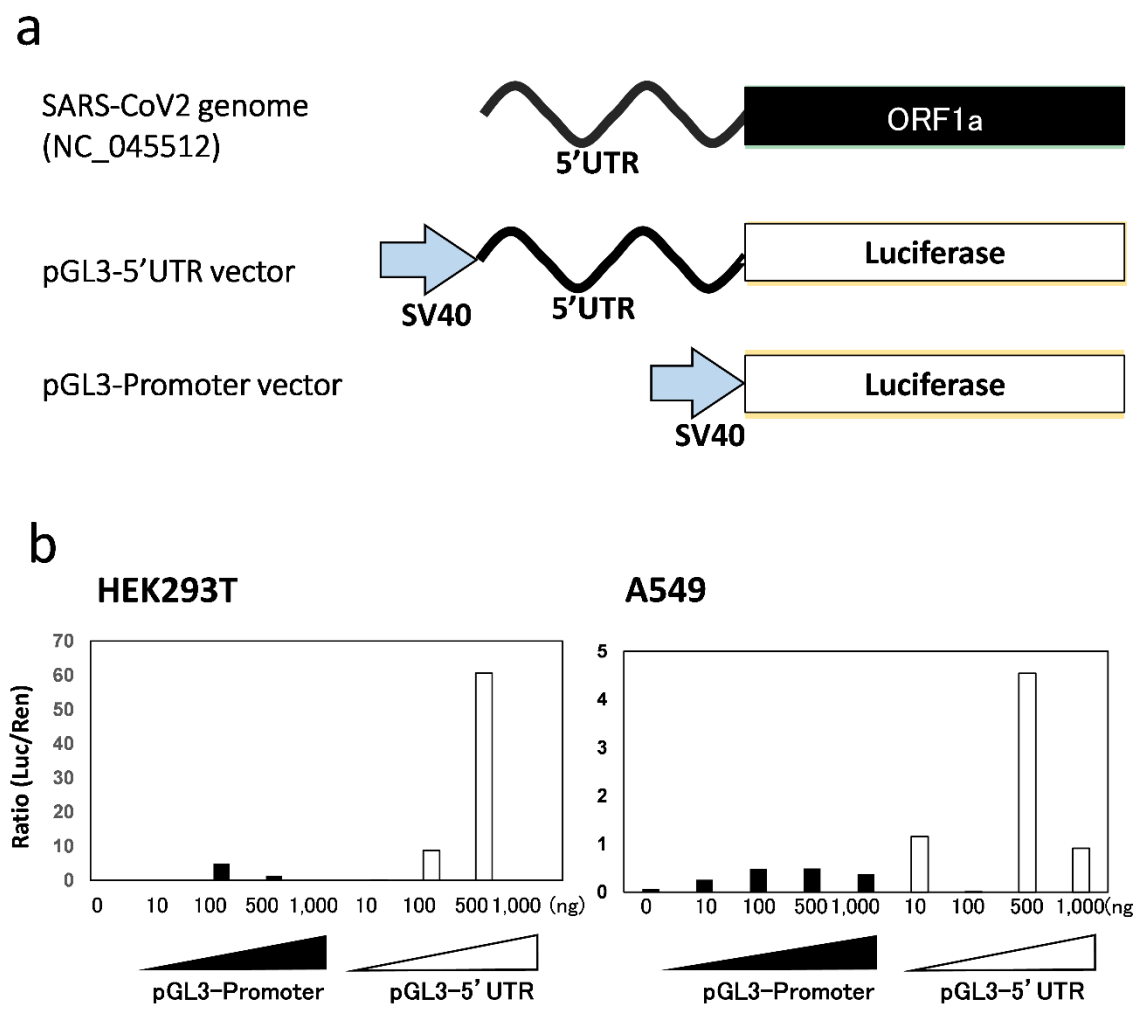

Figure 2. pGL3-5'UTR construct and Luciferase reporter assay. (a) Vector construction with SARS-CoV-2 5'UTR insert in pGL3 luciferase vector. The genomic architecture of SARS-CoV-2 starts with 5' UTR followed by ORF1 and structural genes. To elucidate the translational mechanism in host cells, 5' UTR segment of the SARS- CoV-2 was inserted in the pGL3 vector between SV40 promoter and luciferase gene. Luciferase gene is a reporter

517 for the transfection efficiency and expression of 5’ UTR. Further, luciferase RNA forms the
518 target for crRNA-dCAS13 facilitating Trans immunoprecipitation (TRIP) for 5’UTR bound
519 host translational RNAs. **(b)** Luciferase transcription induced by the SV40 promoter
520 measured as a function of luminescence in HEK293T cells (left) and A549 cells (right).
521 According to the amount of cell introduction, both pGL3-promoter and pGL3-5'UTR vector
522 increased or decreased the activity of luciferase protein. Upon introduction of pGL3-5'UTR
523 vector, relative luciferase activity increased more than 10 times to the equivalent amount of
524 pGL3-promoter. Note that the SARS-CoV-2 derived 5'UTR synergistically activated
525 translation in an intracellular factor-dependent manner. Relative luciferase activity was
526 calculated against the activity of endogenous pRL-RSV serving as control (100%). The
527 Mann-Whitney U test was used for statistical significance ($p < 0.05$).

a

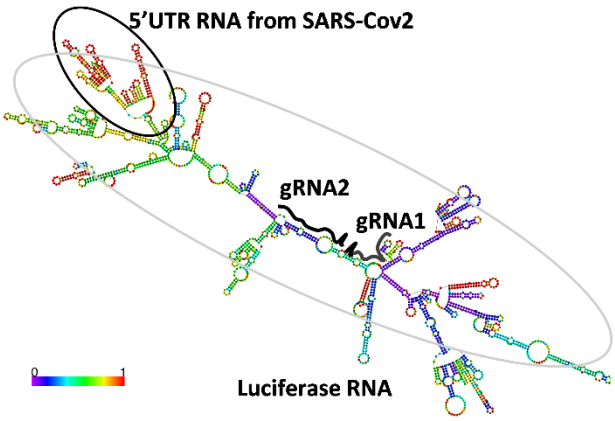
5'UTR RNA from SARS-Cov2
gRNA2
gRNA1
0
1
Luciferase RNA

b

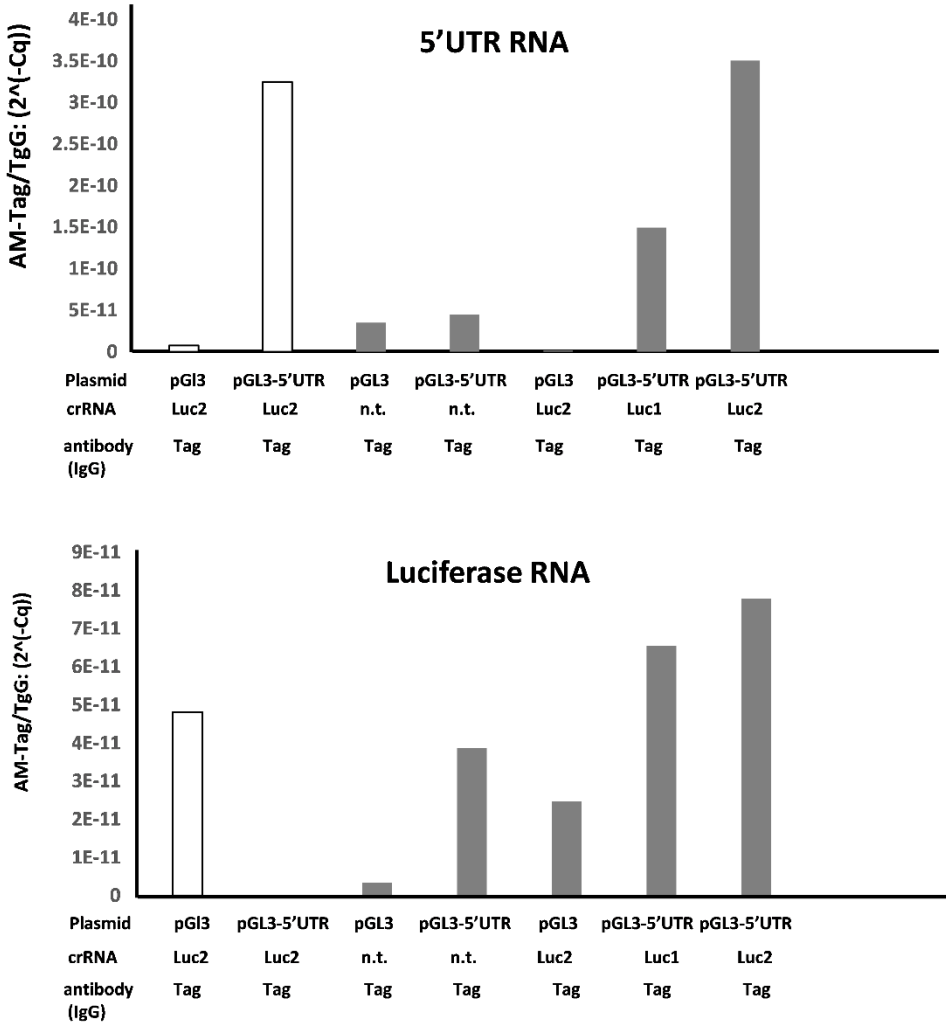
5'UTR RNA
AM-Tag/TgG: (2^(-Cq))
4E-10
3.5E-10
3E-10
2.5E-10
2E-10
1.5E-10
1E-10
5E-11
0
Plasmid pGl3 pGL3-5'UTR pGL3 pGL3-5'UTR pGL3 pGL3-5'UTR pGL3-5'UTR
crRNA Luc2 Luc2 n.t. n.t. Luc2 Luc1 Luc2
antibody (IgG) Tag Tag Tag Tag Tag Tag Tag
Luciferase RNA
AM-Tag/TgG: (2^(-Cq))
9E-11
8E-11
7E-11
6E-11
5E-11
4E-11
3E-11
2E-11
1E-11
0
Plasmid pGl3 pGL3-5'UTR pGL3 pGL3-5'UTR pGL3 pGL3-5'UTR pGL3-5'UTR
crRNA Luc2 Luc2 n.t. n.t. Luc2 Luc1 Luc2
antibody (IgG) Tag Tag Tag Tag Tag Tag Tag

528

Figure 3. RNA-immunoprecipitation. **(a)** Prediction of luciferase mRNA- 5'UTR fusion. Two optimal 28 nt regions gRNAs targeting the luciferase RNA were designed - gRNA1 and gRNA2. **(b)** gRNA-dCas13 mediated RNA immunoprecipitation of host RNA bound to 5'UTR sequences. RT-qPCR was performed to determine the accumulation of immunoprecipitated 5'UTR sequence (Top) and luciferase RNA (bottom) *via* gRNA-dCas13 mediated targeting of luciferase RNA. The host RNA bound to 5'UTR was immunoprecipitated and the enrichment factor was calculated as 2 (-ΔΔCt [RIP / background]). The mean and standard error of the three independent experiments is shown. Statistical analysis was performed using a two-sided paired t-test. * Indicates a significant difference from the control sample at a value of $p < 0.05$.

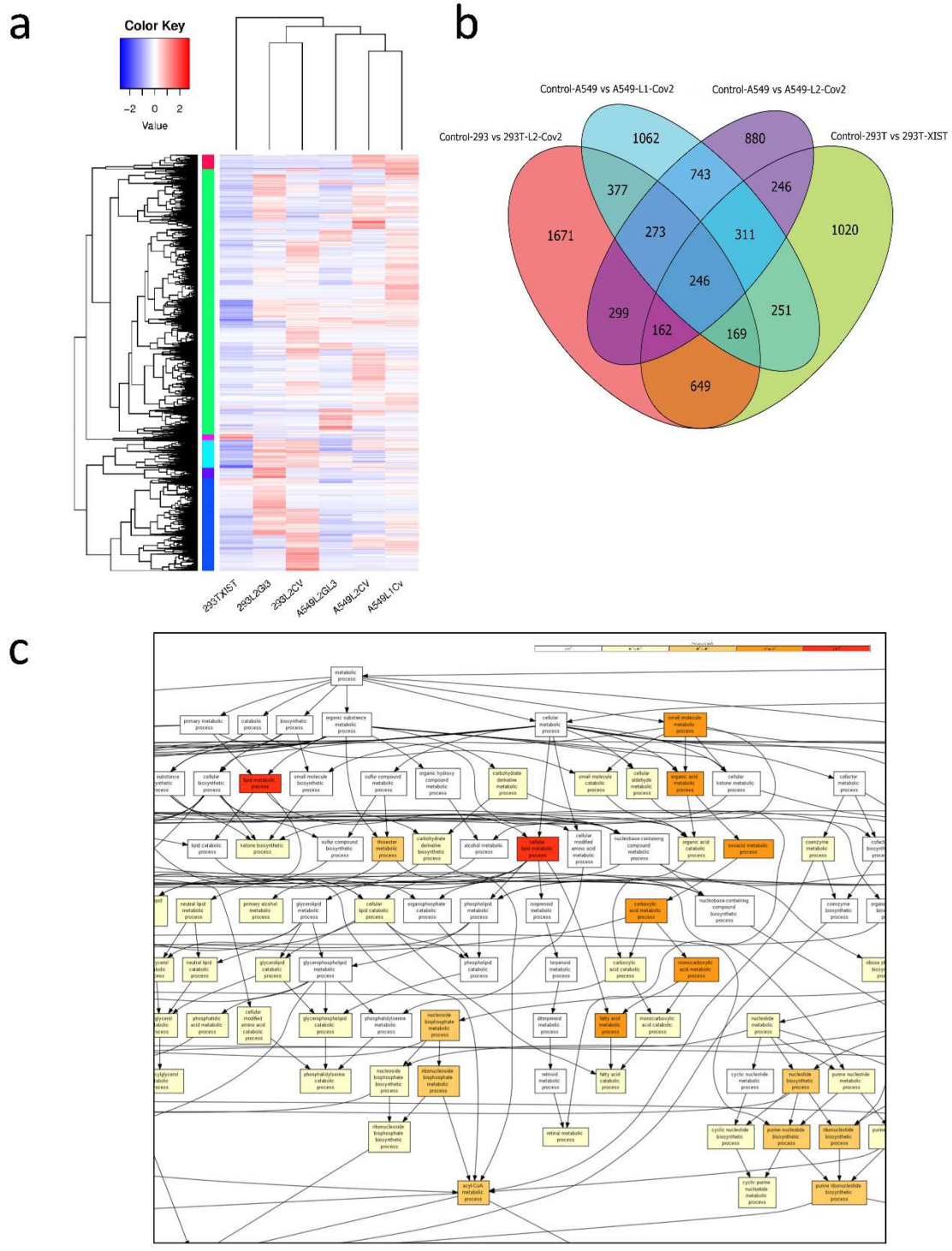

Figure 4. Differential expression by RNA seq analysis. (a) Set of four samples was analyzed for RNA-seq analysis. Each lane is Luciferase RNA-immunoprecipitation sample

543 from no 5'UTR sequence (293L2GL3 and A549L2GL3) and controls, or Luciferase-RNA
544 fused with 5'UTR (293L2CV, A549L2CV, and A549L1Cv) as test samples. (L1 or L2 are
545 guide RNAs targeting Luciferase RNA). Heatmap analysis of differentially enriched genes
546 show enrichment in 293L2CV, A549L2CV, and A549L1CV immunoprecipitated samples.
547 **(b)** Venn diagram showing genes common to the unique genes in the test sample (293L2CV,
548 A549L2CV, and A549L1Cv) that were significantly enriched ($p < 0.05$) compared to the
549 control (293L2GL3 or A549L2GL3). 293T-XIST is an RNA-immunoprecipitation sample
550 serving as a negative control using HEK293T cells expressing lncRNA XIST-targeting guide
551 RNA and dCas13. The genes enriched by Control-293 vs 293T-L2-CoV2, Control-A549 vs
552 A549-L1-CoV2, and Control-A549-L2-CoV2 are human intracellular factors that interact
553 with 5'UTR derived from SARS-CoV-2. **(c)** Genes enriched by Control-293 vs 293T-L2-
554 CoV2 dataset were ranked according to their differential enrichment and the resulting
555 enriched GO terms are visualized using a DAG graphical representation with color-coding
556 reflecting their enrichment degree.
557

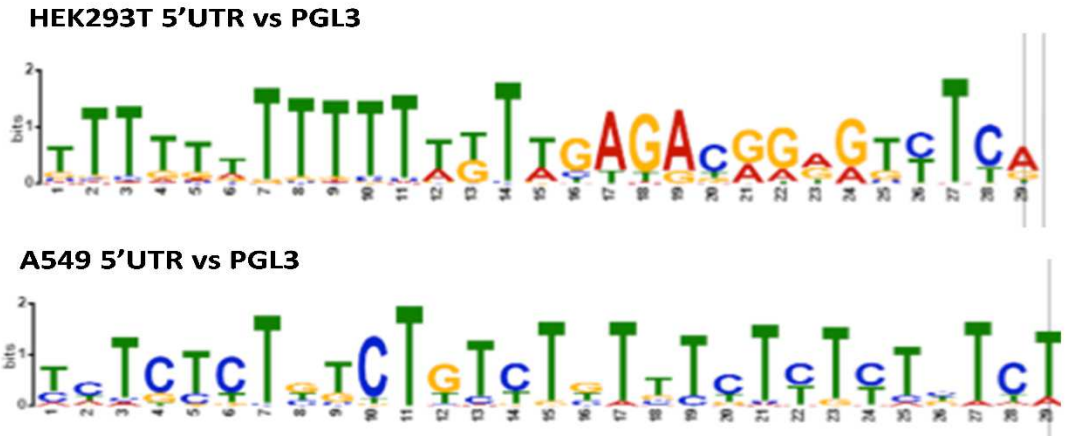

Figure 5. Motif analysis and host binding factors to 5'UTR . The motif in the 5'UTR in HEK293T cells (top) and A549 cells (bottom) is crucial for binding the host translational factors.

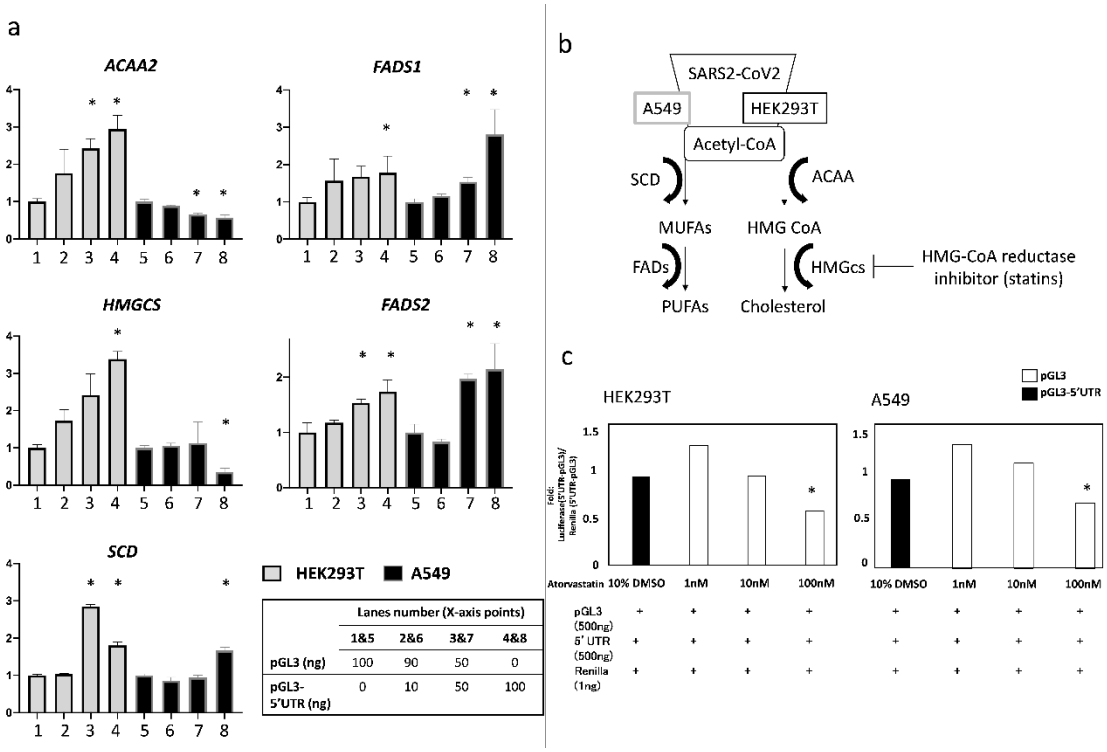

	Lanes number (X-axis points)			
	1&5	2&6	3&7	4&8
pGL3 (ng)	100	90	50	0
pGL3-5'UTR (ng)	0	10	50	100

Figure 6: Overexpression of 5'UTR in SARS-CoV-2 alters genes expression involved in the mevalonate pathway in HEK293T and A549 cells. (a) 1 ug of pGL3-promoter and pGL3-5'UTR vectors were introduced into cells cultured in 6 well plates (0.3×10^6). Expression of lipid metabolism factors from total RNA was measured. Overexpression of 5'UTR affected the expression of ACAA and HMGCS. Results are shown as mean ± SD, and Student's t-test was used as a test of significance. **(b)** Outline of metabolic pathway of Acetyl-CoA by overexpression of 5'UTR of SARS-CoV-2 and inhibitory mechanism of HMG-CoA reductase inhibitors like statins. **(c)** 1 ug of pGL3-promoter and pGL3-5'UTR vectors was introduced in cells cultured in 24 well plates. HMGCoA reductase inhibitors were added to the culture solution at a concentration range of 1nM, 10nM, 100nM and 1,000 nM. Following incubation for 48 hours, the luciferase activity was measured. To assess the effect on the 5'UTR, the pGL3-promoter and luciferase activity from each adjacent well into which the pGL3-5'UTR vector was introduced were subtracted. The internal control used was the sum of each value. The results were shown as mean ± SD and were tested for significance by Student's t-test. The internal control used was the sum of the respective values. Results were shown as mean ± SD, and Student's t-test examined significance.

List of Tables

Table 1. Top 10 Gene ontology terms enriched for binding 5'UTR of SARS-CoV-2.

GO term	Description	P-value	FDR q-value
GO:0044255	Cellular lipid metabolic process	5.29E-11	5.58E-07
GO:0006629	Lipid metabolic process	4.56E-10	2.41E-06
GO:0032787	Monocarboxylic acid metabolic process	2.05E-09	7.22E-06
GO:0019752	Carboxylic acid metabolic process	1.07E-08	2.81E-05
GO:0006082	Organic acid metabolic process	1.07E-08	2.25E-05
GO:0044281	Small molecule metabolic process	2.85E-08	5.01E-05
GO:0006631	Fatty acid metabolic process	3.53E-08	5.31E-05
GO:0043436	Oxoacid metabolic process	4.95E-08	6.53E-05
GO:0050690	Regulation of defense response to virus by virus	2.77E-07	3.25E-04
GO:0006637	Acyl-CoA metabolic process	3.05E-07	3.22E-04

Table 2. Host factors binding via consensus recognition motif to 5' UTR of SARS- CoV-2.

Host Proteins	Recognition Motif in 5' UTR	K-mer	Z-score P-value (HEK293T)	Z-score P-value (A549)
RBM38	gggugug	4.321	7.77E-06	8.43E-08
BRUNOL5	uguguau	3.912	4.58E-05	6.64E-08
BRUNOL4	uguguau	3.838	6.20E-05	9.77E-06

TARDBP	ugugug	3.826	6.51E-05	1.38E-06

591

592

Figures

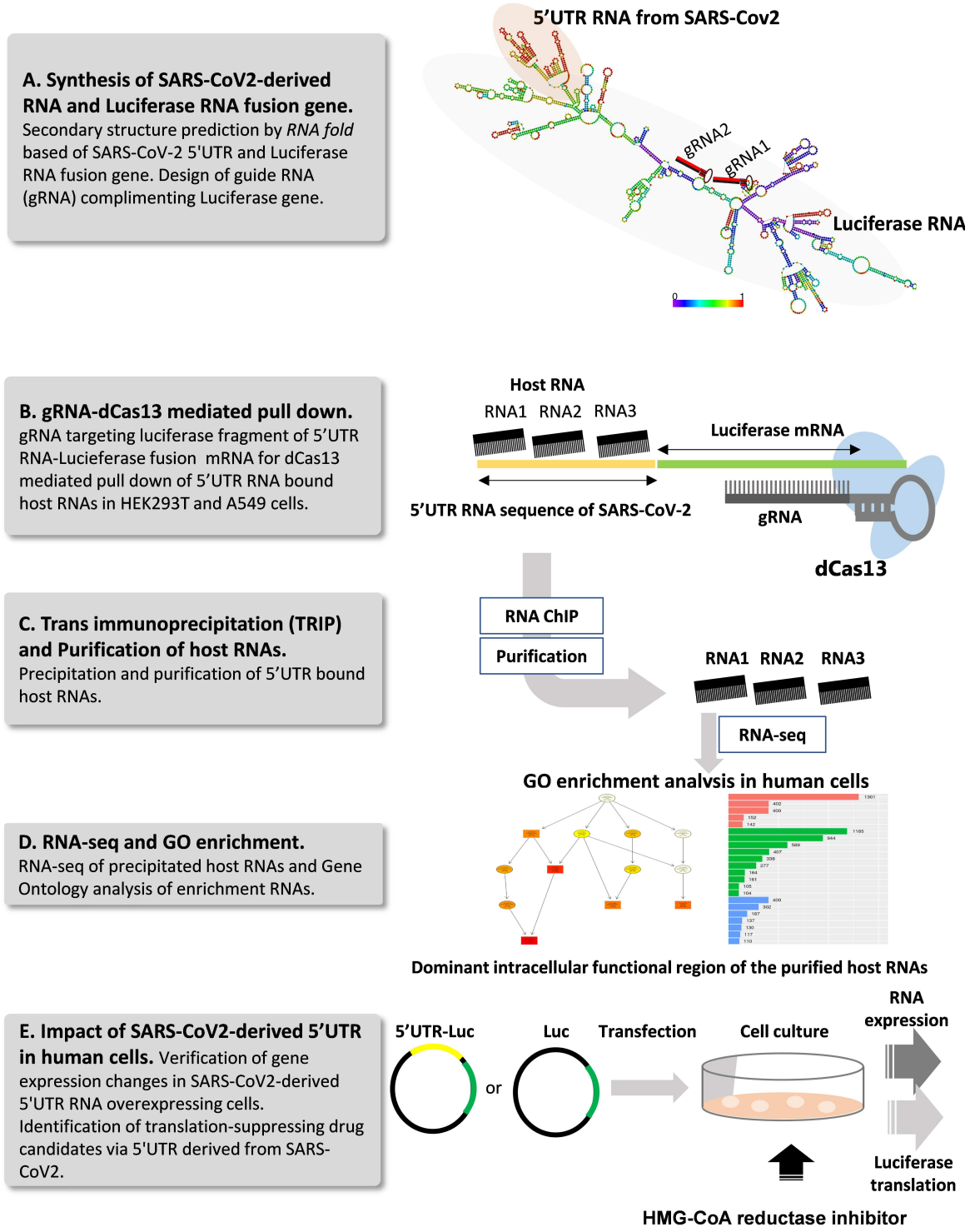

Figure 1

Workflow of the study.

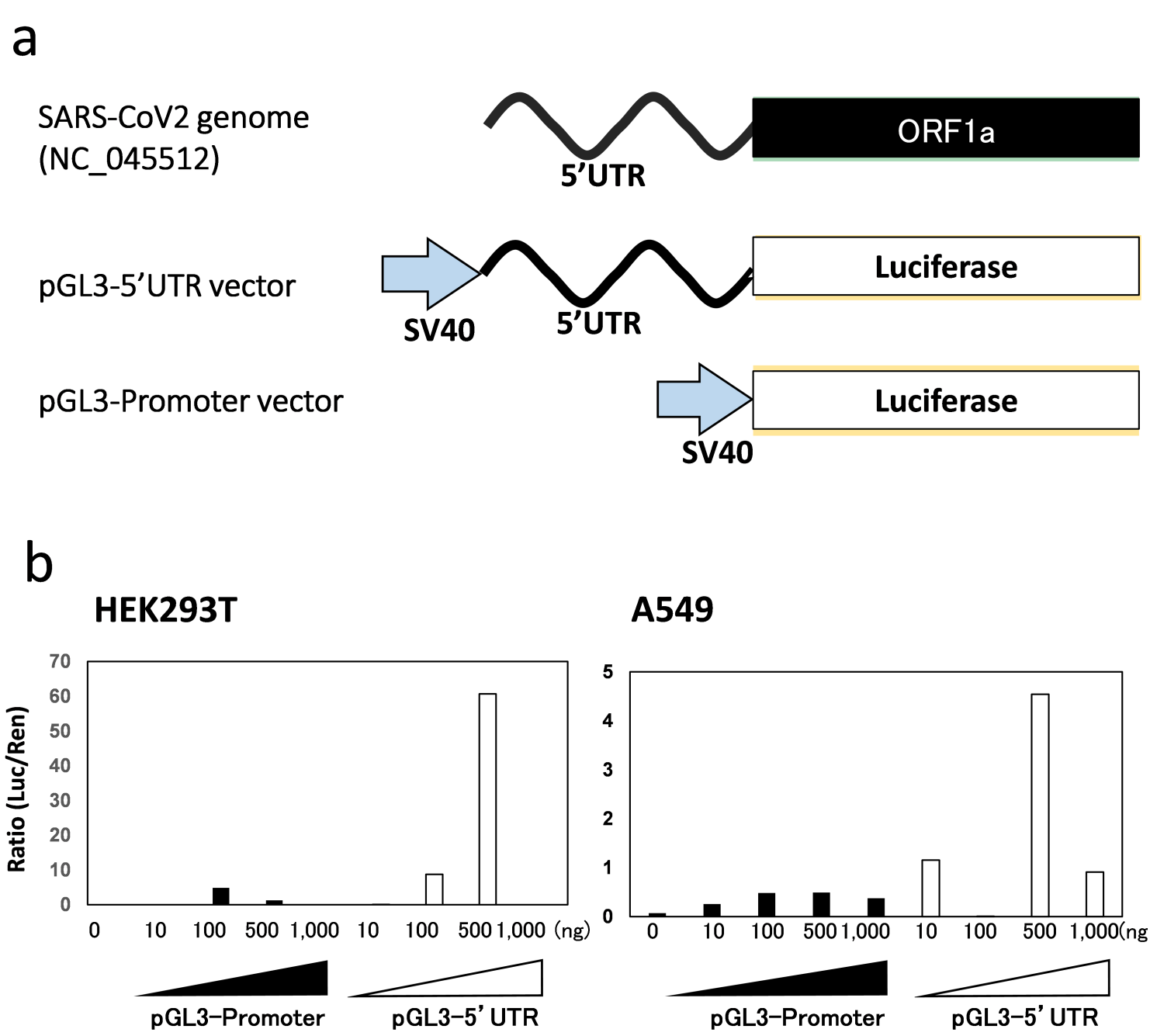

Figure 2

pGL3-5'UTR construct and Luciferase reporter assay. (a) Vector construction with SARS-CoV-2 5'UTR insert in pGL3 luciferase vector. The genomic architecture of SARS-CoV-2 starts with 5' UTR followed by ORF1 and structural genes. To elucidate the translational mechanism in host cells, 5' UTR segment of the SARS- CoV-2 was inserted in the pGL3 vector between SV40 promoter and luciferase gene. Luciferase gene is a reporter 34 for the transfection efficiency and expression of 5' UTR. Further, luciferase RNA forms the target for crRNA-dCAS13 facilitating Trans immunoprecipitation (TRIP) for 5'UTR bound host translational RNAs. (b) Luciferase transcription induced by the SV40 promoter measured as a function of luminescence in HEK293T cells (left) and A549 cells (right). According to the amount of cell introduction, both pGL3-promoter and pGL3-5'UTR vector increased or decreased the activity of luciferase protein.

Upon introduction of pGL3-5'UTR vector, relative luciferase activity increased more than 10 times to the equivalent amount of pGL3-promoter. Note that the SARS-CoV-2 derived 5'UTR synergistically activated translation in an intracellular factor-dependent manner. Relative luciferase activity was calculated against the activity of endogenous pRL-RSV serving as control (100%). The Mann-Whitney U test was used for statistical significance ($p < 0.05$).

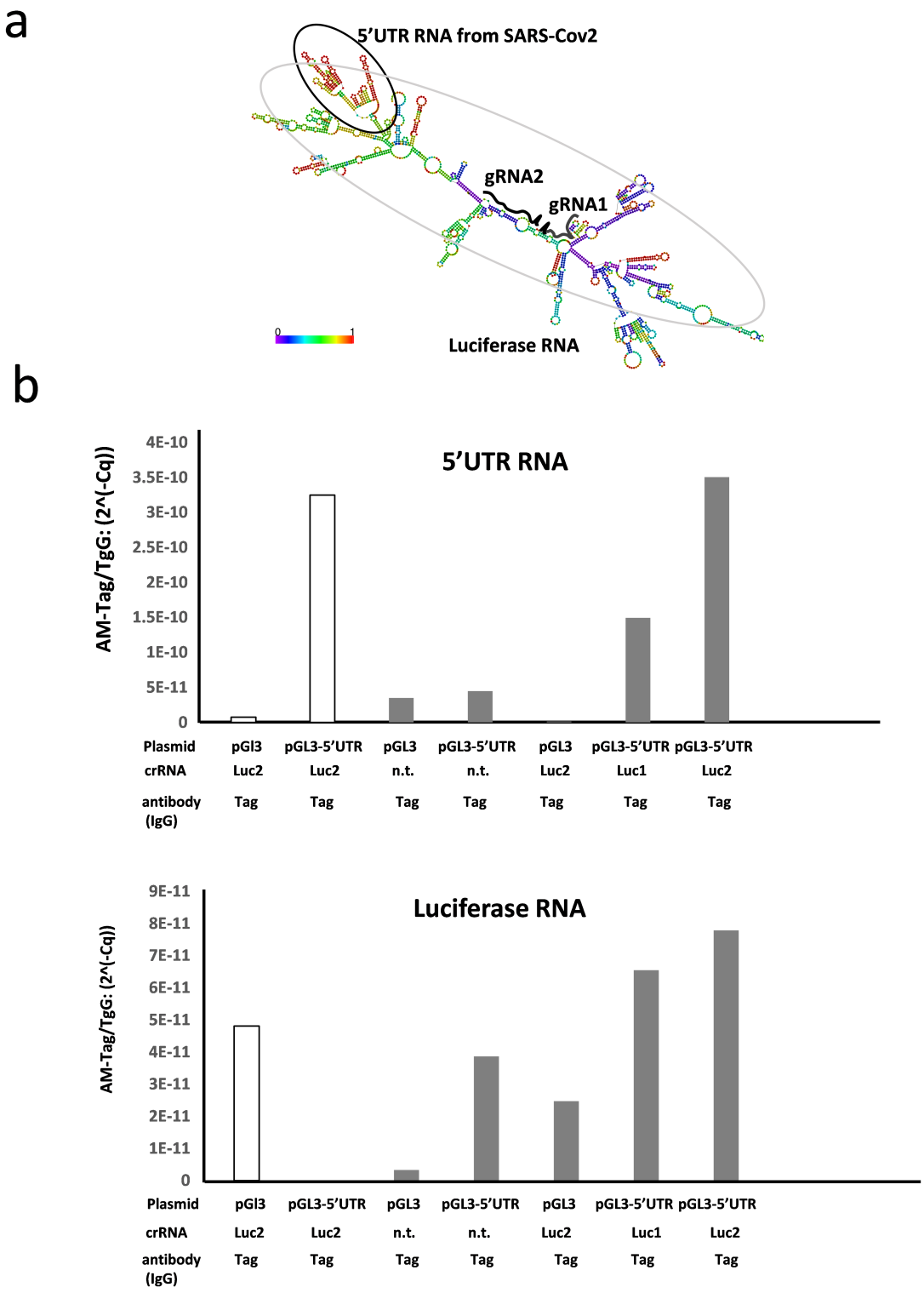

Figure 3

RNA-immunoprecipitation. (a) Prediction of luciferase mRNA- 5'UTR fusion. Two optimal 28 nt regions gRNAs targeting the luciferase RNA were designed - gRNA1 and gRNA2. (b) gRNA-dCas13 mediated RNA immunoprecipitation of host RNA bound to 5'UTR sequences. RT-qPCR was performed to determine the accumulation of immunoprecipitated 5'UTR sequence (Top) and luciferase RNA (bottom) via gRNA-dCas13 mediated targeting of luciferase RNA. The host RNA bound to 5'UTR was immunoprecipitated and the enrichment factor was calculated as 2 (-ΔΔCt [RIP / background]). The mean and standard error of the three independent experiments is shown. Statistical analysis was performed using a two-sided paired t-test. * Indicates a significant difference from the control sample at a value of $p < 0.05$.

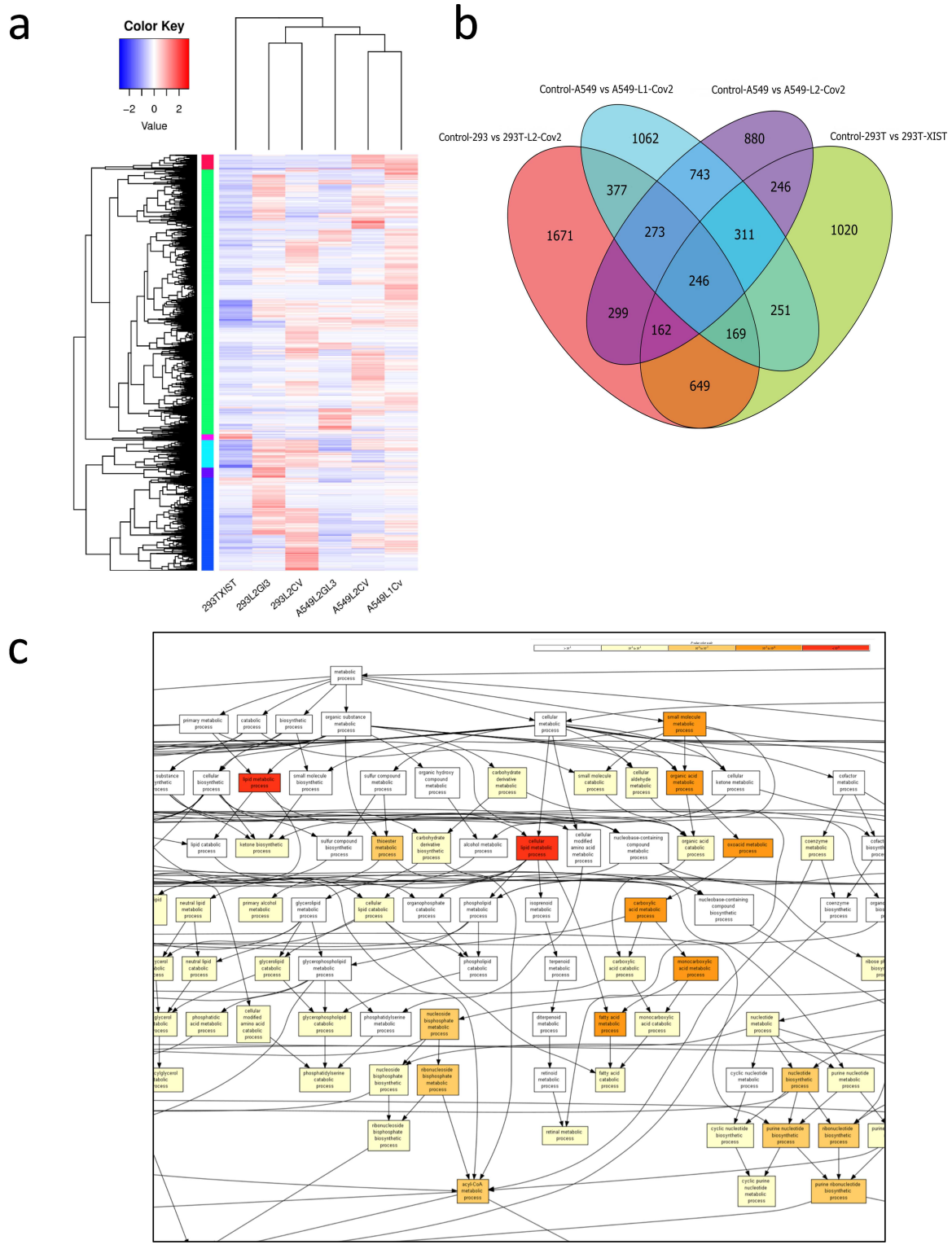

Figure 4

Differential expression by RNA seq analysis. (a) Set of four samples was analyzed for RNA-seq analysis. Each lane is Luciferase RNA-immunoprecipitation sample 38 from no 5'UTR sequence (293L2GL3 and A549L2GL3) and controls, or Luciferase-RNA fused with 5'UTR (293L2CV, A549L2CV, and A549L1Cv) as test samples. (L1 or L2 are guide RNAs targeting Luciferase RNA). Heatmap analysis of differentially enriched genes show enrichment in 293L2CV, A549L2CV, and A549L1CV immunoprecipitated samples.

(b) Venn diagram showing genes common to the unique genes in the test sample (293L2CV, A549L2CV, and A549L1Cv) that were significantly enriched (p <0.05) compared to the control (293L2GL3 or A549L2GL3). 293T-XIST is an RNA-immunoprecipitation sample serving as a negative control using HEK293T cells expressing lncRNA XIST-targeting guide RNA and dCas13. The genes enriched by Control-293 vs 293T-L2-CoV2, Control-A549 vs A549-L1-CoV2, and Control-A549-L2-CoV2 are human intracellular factors that interact with 5'UTR derived from SARS-CoV-2. (c) Genes enriched by Control-293 vs 293T-L2-CoV2 dataset were ranked according to their differential enrichment and the resulting enriched GO terms are visualized using a DAG graphical representation with color-coding reflecting their enrichment degree.

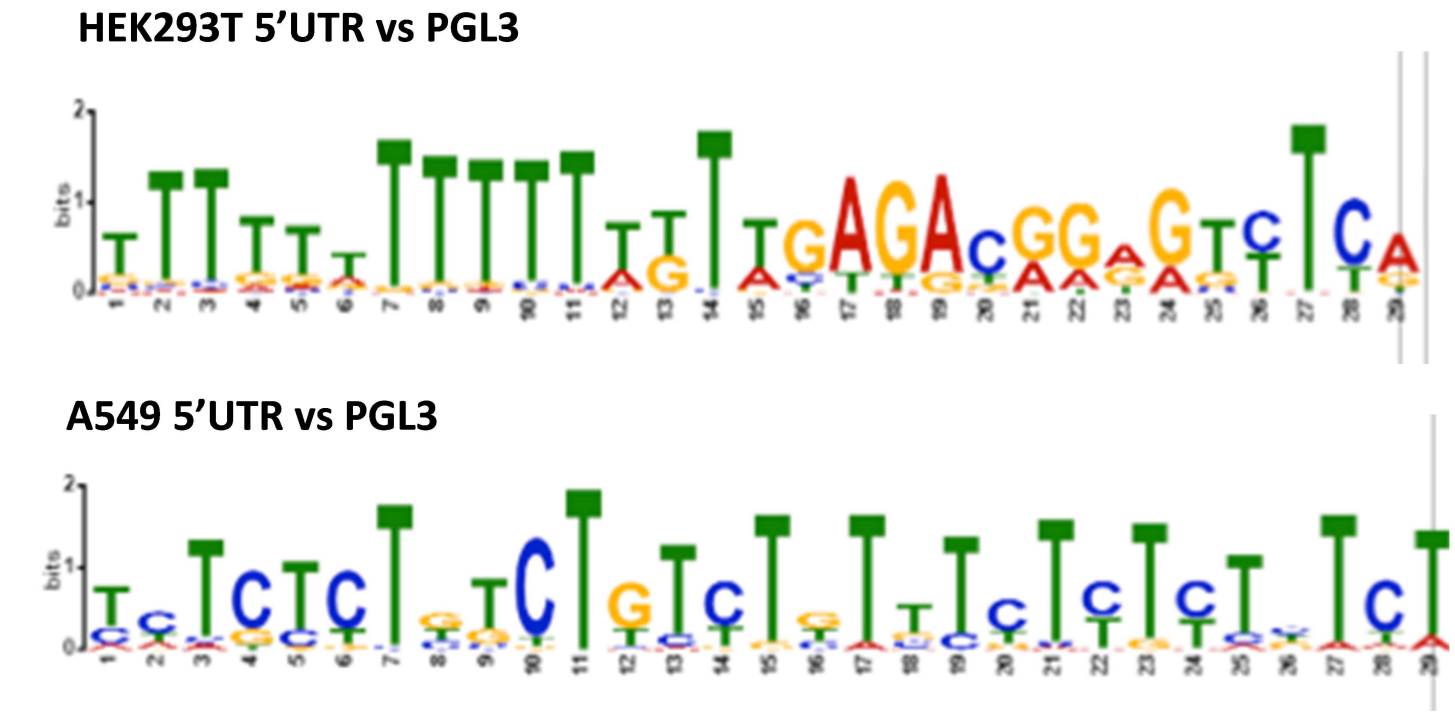

Figure 5

Motif analysis and host binding factors to 5’UTR . The motif in the 5’UTR in HEK293T cells (top) and A549 cells (bottom) is crucial for binding the host translational factors.

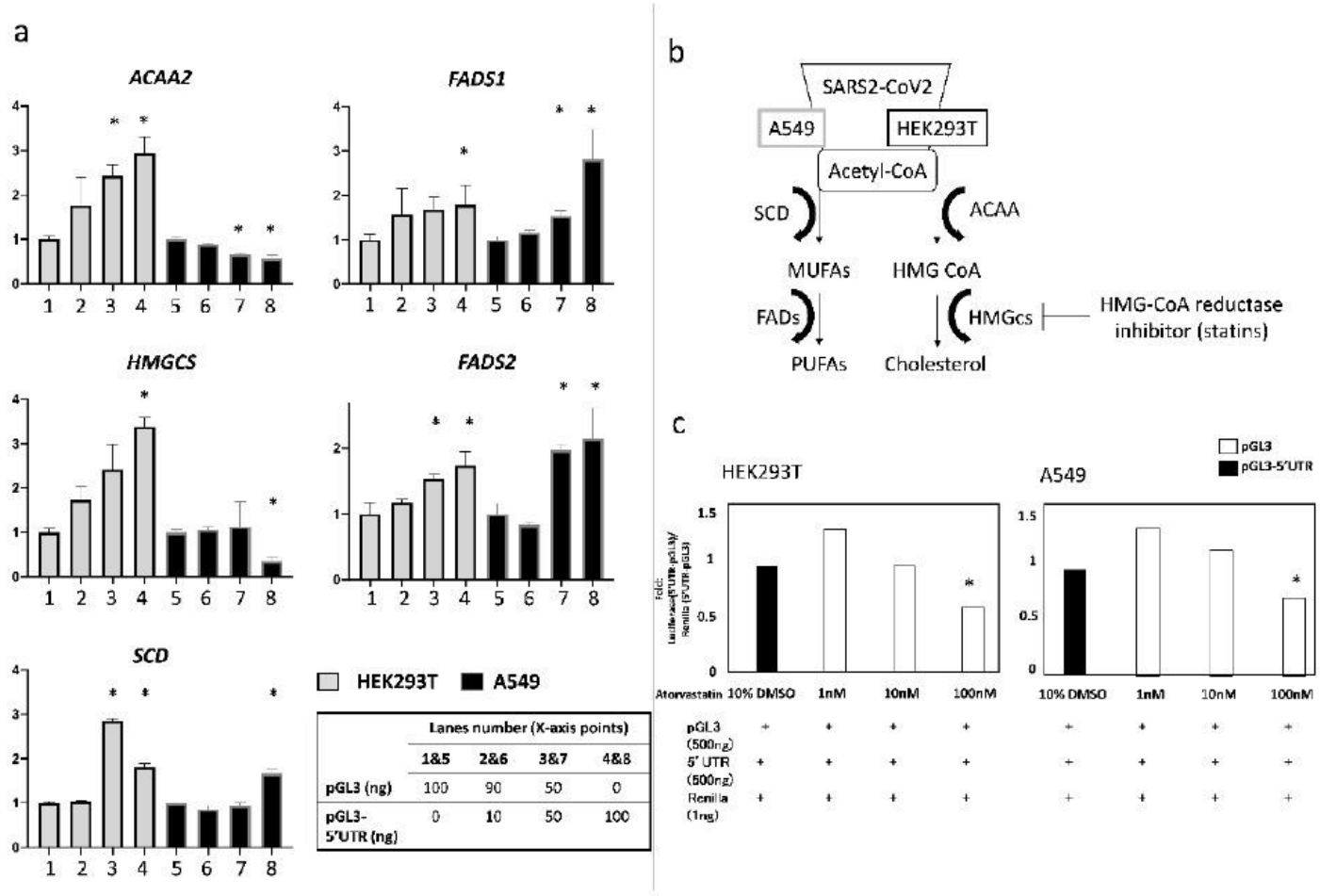

Figure 6

Overexpression of 5'UTR in SARS-CoV-2 alters genes expression involved in the mevalonate pathway in HEK293T and A549 cells. (a) 1 ug of pGL3-promoter and pGL3-5'UTR vectors were introduced into cells cultured in 6 well plates (0.3 x 106). Expression of lipid metabolism factors from total RNA was measured. Overexpression of 5'UTR affected the expression of ACAA and HMGCS. Results are shown as mean ± SD, and Student's t-test was used as a test of significance. (b) Outline of metabolic pathway of Acetyl- CoA by overexpression of 5'UTR of SARS-CoV-2 and inhibitory mechanism of HMG-CoA reductase inhibitors like statins. (c) 1 ug of pGL3-promoter and pGL3-5'UTR vectors was introduced in cells cultured in 24 well plates. HMGCoA reductase inhibitors were added to the culture solution at a concentration range of 1nM, 10nM, 100nM and 1,000 nM. Following incubation for 48 hours, the luciferase activity was measured. To assess the effect on the 5'UTR, the pGL3-promoter and luciferase activity from each adjacent well into which the pGL3-5'UTR vector was introduced were subtracted. The internal control used was the sum of each value. The results were shown as mean ± SD and were tested for significance by Student's t-test. The internal control used was the sum of the respective values. Results were shown as mean ± SD, and Student's t-test examined significance.

Supplementary Files

This is a list of supplementary files associated with this preprint. Click to download.

- TABLES.pdf
- Supplementalfigure.pdf
- Supplementalfigure.pdf